Structural Safety 78 (2019) 33–47

Contents lists available at ScienceDirect

Structural Safety

journal homepage: www.elsevier.com/locate/strusafe

Societal risk assessment of transportation networks under uncertainties due to climate change and population growth

David Y. Yang, Dan M. Frangopol*

Department of Civil and Environmental Engineering, ATLSS Engineering Research Center, Lehigh University, Bethlehem, PA, USA

ARTICLE INFO

Keywords:
Climate change
Population growth
Transportation network
Robust traffic assignment
Risk assessment

ABSTRACT

Climate change and population growth can affect the supply and the demand sides of transportation networks, respectively. Rational assessment of societal risk of transportation networks should consider these effects, both of which are uncertain in nature. In this paper, a novel method is proposed to assess societal risk of transportation networks subjected to uncertainties due to climate change and future population growth. The method is posited on a robust traffic assignment model using the expected residual minimization approach. A novel algorithm, combining smoothing method, quasi-Newton technique, and Latin hypercube sampling, is developed for the efficient implementation of the proposed method. The proposed method can produce a deterministic traffic flow pattern that deviates as little as possible from the traffic flow patterns associated with all future scenarios. The obtained traffic flow pattern can then be used to estimate societal risk of transportation networks. A number of examples, including a real-world highway bridge network in Camden County, New Jersey, are provided in this paper to demonstrate the efficiency, effectiveness, and application of the proposed method. It is found from the examples that (a) the proposed method is more efficient and robust than existing algorithms for robust traffic assignment under uncertainties, and (b) climate change and population growth can significantly alter the traffic pattern in a transportation network and thus increase the societal risk posed upon traffic users.

1. Introduction

Climate change is liable for the increasingly frequent and intensified hydrometeorological hazards and the acceleration of deterioration of transportation networks [1]. Population growth is responsible for the increase in traffic demands of transportation networks. In this paper, a novel approach is proposed to efficiently evaluate the societal risk of transportation networks under climate change and population growth. The emphasis is on the riverine flooding hazards to deteriorating bridges and their associated transportation networks, although this approach can also be used to consider other climate-related hazards such as hurricanes and other transportation network components such as pavement. Given the complex relation between climate change and population growth [2], hazard conditions and population growth are assumed herein to be independent.

For transportation networks, traffic assignment models are usually used to predict traffic flow. Based on Wardrop's user equilibrium, traffic assignment in general deals with an underlying interaction between traffic demand and traffic supply [3]. The traffic demand is the traffic users traveling between a number of origin-destination (OD) pairs; the traffic supply refers to the capacities of physical assets of transportation infrastructure, mostly defined by flow-delay functions associated with links in a transportation network. For transportation networks under climate change and population growth, both traffic supply and traffic demand become uncertain due to the existence of multiple plausible future scenarios. Specifically, on the supply side, extreme hazards induced by climate change can compromise network capacities, whereas, on the demand side, population growth indicates that more traffic users will travel between OD pairs.

Although few studies have considered transportation network performance under climate change and population growth, uncertainties in general have been investigated in the fields of transportation network analysis and infrastructure management. It should be noted that supply and demand uncertainties considered herein are different from the uncertainties of traffic users' perceptions of travel costs, which have been conventionally studied under the framework of stochastic traffic assignment [4,5]. In the context of traffic assignment, supply and demand uncertainties can be categorized as short-term uncertainties and long-term uncertainties. The former are usually induced by short-term events such as accidents and/or adverse weather conditions, which disturb the network performance in a relatively short period (e.g. during the travel of traffic users). A key feature of short-term

* Corresponding author.
E-mail address: dan.frangopol@lehigh.edu (D.M. Frangopol).

https://doi.org/10.1016/j.strusafe.2018.12.005
Received 16 April 2018; Received in revised form 7 December 2018; Accepted 13 December 2018
Available online 04 January 2019
0167-4730/ © 2018 Elsevier Ltd. All rights reserved.

uncertainties is that traffic users have no or little information of these short-term events when they are planning their trips. The latter are induced by events that have a long-term impact to the transportation network (e.g. closure of links due to failure or maintenance). Since the duration of these events is much longer than any single journey within the network, a new equilibrium state of traffic flow will form. Different from short-term uncertainties, traffic users in a transportation network subjected to long-term uncertainty can still be assumed to have complete or nearly complete information during the planning of their trips.

Existing studies of short-term uncertainties are mainly on the immediate changes in the behavior of traffic users and the instant effects on the transportation network and traffic users, e.g. dynamic traffic assignment [6], formation of queues [7], and travel time reliability [8]. By contrast, studies of long-term uncertainties mostly are related to problems with a much longer time horizon, e.g. maintenance planning for deteriorating pavements and bridges [9–13], risk assessment and risk mitigation of networks under hazards [14,15], and restoration of infrastructure systems after hazards [16,17]. In these cases, changes of network properties are considered to be persistent, while a new static equilibrium can be established shortly after the change (compared to time horizon under investigation).

The present study is focused on the long-term uncertainties arising from climate change and population growth. Most of the aforementioned studies on long-term uncertainties are ad hoc studies for certain types of hazards and structures. Therefore, despite a relatively large number of studies, there is a lack of general and efficient methods to deal with long-term uncertainties. In addition, none of the aforementioned studies took into account climate change and future population growth in their analyses. The present study proposes a general method for societal risk assessment of transportation networks under uncertainties due to climate change and population growth. The proposed method is underpinned by a robust traffic assignment model formulated using the expected residual minimization (ERM) approach [18]. Despite the uncertain future scenarios associated with climate change and population growth, robust traffic assignment is able to provide a deterministic equilibrium pattern that deviates as little as possible from the equilibrium states of all possible scenarios. This deviation can lead to an error in the estimated risk if a specific future scenario materializes. This error may further propagate to the potential management plan generated based on the estimated risk, which will cause regret felt by the decision-maker [19]. However, given that realization of any future scenario is not sure, the proposed approach can still assist with decision-making by generating plans with low regret despite the inevitability of errors. In summary, using the obtained robust traffic pattern, risk assessment and the potential risk management assimilates conceptually to the scenario-based management with robust optimization under minimax regret criterion [19].

To present the proposed method, the paper is organized as follows: in the following section, it is first explained how future climate change and population growth can be converted into future conditions of network supply and demand; the formulation of robust traffic assignment model based on the ERM approach is then described; a novel algorithm is presented for efficient implementation of robust traffic assignment; subsequently, it is shown how the flow pattern obtained from robust traffic assignment can be used for societal risk assessment. A number of examples are provided to demonstrate the efficiency, effectiveness, and application of the proposed method.

2. Modeling of future scenarios

As stated previously, both the future condition of and the future demand on transportation networks involve uncertainties due to climate change and population growth. In order to determine a robust traffic pattern, future scenarios of climate change and population growth should be first identified.

On the supply side, climate change can affect transportation infrastructure such as bridges and pavements through gradual deterioration due to environmental aggression and sudden capacity drop due to natural hazards. For the former, climate change is likely to accelerate deterioration of infrastructure components [1,20,21]; for the latter, the frequency and intensity of hydrometeorological hazards (e.g. flooding and hurricanes) increase due to climate change and its derived effects (e.g. global warming, sea level rise, and intense precipitation). It should be noted that changes in gradual deterioration and natural hazards are likely to be highly correlated due to their common source from climate change. For instance, higher temperature, sea level rise, and intense precipitation not only accelerate the deterioration process, but also exacerbate extreme flooding and hurricanes [1,22]. Modeling of climate change should be capable of identifying scenarios that include all relevant consequences of climate change. On the demand side, population growth can result in the increase of travel demand and the alteration of land uses. In this paper, future OD demands are determined based on the rates of population growth [23].

Combining the future scenarios of climate change and those of population growth, the overall future scenarios can be obtained. For example, if climate change effects can lead to three cases of deterioration rates and extreme flooding characterized by annual maximum streamflow, and future population growth has two possible paths, then there are in total $3 \times 2 = 6$ scenarios, as indicated in Fig. 1, to be considered in robust traffic assignment. It should be noted that population growth might to some extent be contingent upon future climate change scenarios. Therefore, conditional probabilities given different climate change scenarios are needed to determine the joint probabilities of overall future scenarios. This process is illustrated in Fig. 1.

Unlike population growth, which can be reflected by directly increasing OD demands, scenario parameters associated with climate change (e.g. the deterioration rate and streamflow) need to be converted to road properties in order to consider them in robust traffic assignment. In general, all components in transportation networks (e.g. pavements and bridges) are likely to deteriorate and fail under harsh environments and natural hazards. Deterioration of pavements is characterized by the increase in road roughness and the development of cracks on road surface. These detrimental effects will lower the free speed of vehicles, compromise the comfort of passengers, increase fuel consumptions, and even affect route choices of traffic users [9,24–26]. For instance, the free speed on a highway link can be related to the roughness of the road by the following equation [25]:

$$v = v_0 - 0.0034 \cdot \mathrm{UI} \tag{1}$$

where v is the free speed on a deteriorating link (km/h); v_0 is the original free speed on a link (km/h); and UI is the unevenness index (mm/km) quantifying the pavement roughness. Deterioration of bridges compromises bridge functionality, serviceability, and structural safety. Bridge failure due to deterioration can dramatically reduce the link capacities and increase the link length due to detours. For a bridge under relevant hazards, its condition (safe or failed) can be represented by a Bernoulli random variable. The probability of failure can then be determined using structural reliability methods. When failing bridges are present in a link, link capacities can be adjusted as follows [27]:

$$t_a^0 = \frac{s_{a,0} + \sum s_i}{v_a} \tag{2}$$

$$C_a = C_{a,0} \cdot (1 - \max d_i) \tag{3}$$

where t_a^0 is the free speed travel time; v_a is the free speed on link a; $s_{a,0}$ is the original link length; $\sum s_i$ is the sum of detour lengths of all failing bridges; C_a is the link capacity with failing bridges; $C_{a,0}$ is the original link capacity without any failing bridges; and $\max d_i$ is the drop in link capacity due to bridge failure. It should be noted that Eq. (3) is often used for highway bridge networks located in urban regions, where detours in the form of local roads are usually available in the case of a bridge failure. Nevertheless, these detours can considerably reduce the

Future scenarios	Scenario probability*	Scenario parameters		
S_1	$P_{s1} = P_{C1} \cdot \Pr[G_1 \mid C_1]$	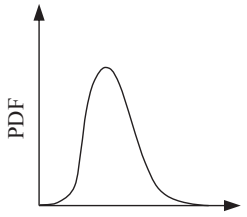	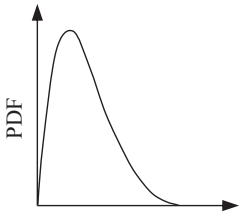	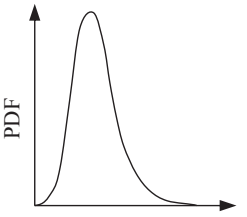
S_2	$P_{s2} = P_{C1} \cdot \Pr[G_2 \mid C_1]$	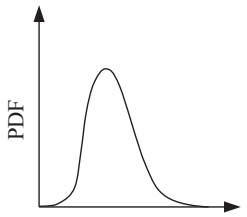	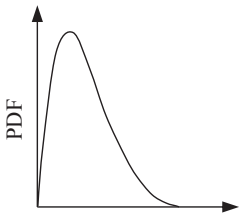	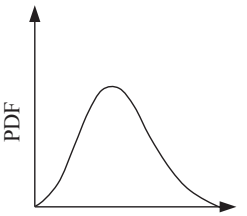
S_3	$P_{s3} = P_{C2} \cdot \Pr[G_1 \mid C_2]$	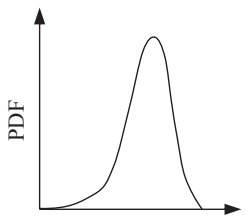	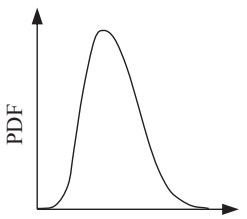	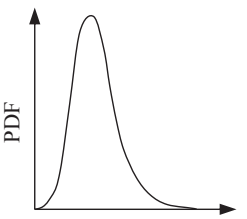
S_4	$P_{s4} = P_{C2} \cdot \Pr[G_2 \mid C_2]$	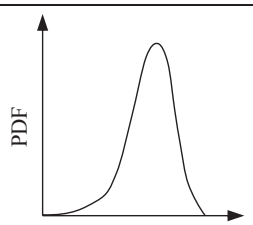	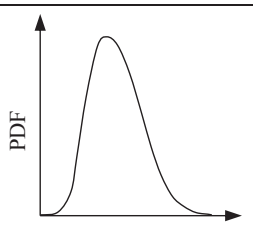	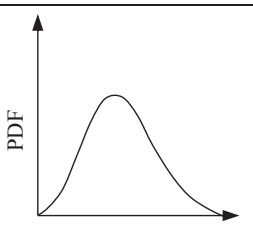
S_5	$P_{s5} = P_{C3} \cdot \Pr[G_1 \mid C_3]$	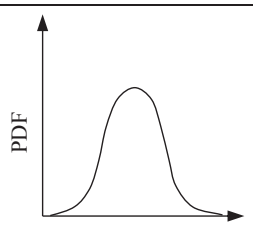	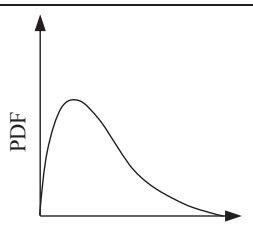	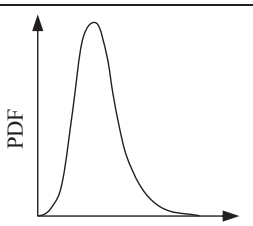
S_6	$P_{s6} = P_{C3} \cdot \Pr[G_2 \mid C_3]$	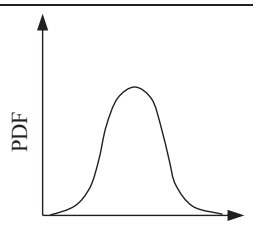	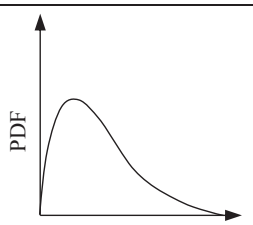	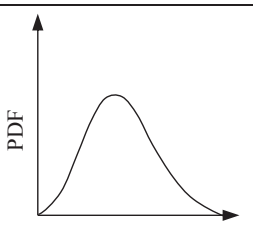
		Deterioration rate	Annual maximum streamflow	OD demands

* Note: Conditional probabilities are needed to evaluate scenario probabilities; $\Pr[G_1 \mid C_1]$ represents the conditional probability of the occurrence of population growth scenario G_1 given the occurrence of climate change scenario C_1.

Fig. 1. Example of future scenarios considering climate change and population growth.

link capacity. The bottleneck of the link is decided by the maximum among link capacity drops associated with the detours of all failing bridges. If all roads (including highways and local roads) are considered or a detour is not available, a sufficiently small value can be assigned to represent the link capacity if any bridge on the link fails. This is equivalent in computational sense to removing that link from the network. For a transportation network comprised of multiple bridges (i.e. a bridge network), failure patterns of all relevant bridges, including how many and which bridges have failed, can be formulated as mutually exclusive and collectively exhaustive events. The occurrence probabilities of these events can be represented by system reliability problems and solved using existing system reliability methods or simulation techniques [27,28]. Therefore, the supply uncertainties of a bridge network, i.e. the probabilities of different network configurations (e.g. networks with different failing bridges), are quantified by a probability mass function (PMF) depending on bridge failure patterns and the corresponding link properties.

To summarize, identification of future scenarios can be conducted

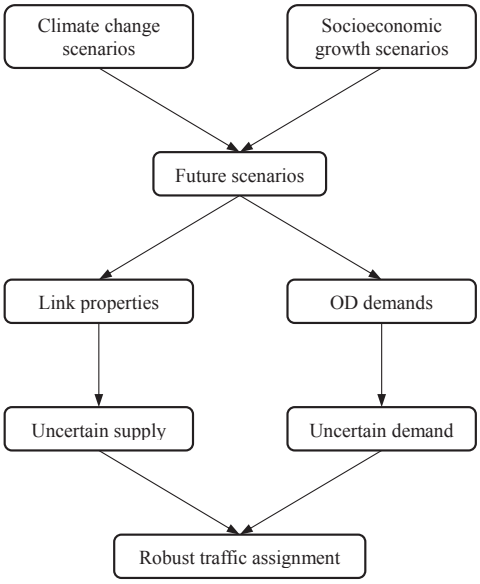

Fig. 2. Preparation for robust traffic assignment.

following the flowchart in Fig. 2. First, different future scenarios are identified for climate change and population growth, respectively. For each scenario, probabilistic link properties and OD demands, representing supply and demand uncertainties, are derived and provided as input for the robust traffic assignment model described in the following section.

3. Robust traffic assignment under demand and supply uncertainties

3.1. Symbols and definitions

To facilitate the following discussion, symbols and notations are firstly defined. For a set $\mathscr{S}$, $|\mathscr{S}|$ is used to denote the cardinality of $\mathscr{S}$. For a random variable X, $\mathbb{E}[X]$, and $\mathbb{P}(x)$ are the expected value of X and the probability of occurrence of the event $\{E: X = x\}$. Now suppose there is a transportation network represented by a graph model $\mathscr{G} = (\mathscr{N}, \mathscr{A})$, where $\mathscr{N}$ is the set of all nodes in the network and $\mathscr{A}$ is the set of all links connecting these nodes. The set of OD pairs in the network is denoted by $\mathscr{C}$, and the set of all routes with respect to all OD pairs is denoted by $\mathscr{R}$. The result of traffic assignment can be represented as a route flow pattern or as a link flow pattern, denoted herein by $\mathbf{h} \in \mathbb{R}^{|\mathscr{R}|}$ and $\mathbf{f} \in \mathbb{R}^{|\mathscr{A}|}$, respectively. The relation between $\mathbf{h}$ and $\mathbf{f}$ can be expressed as [5]

$$\mathbf{f} = \Delta\mathbf{h} \tag{4}$$

where $\Delta = (\delta_{a,r}) \in \mathbb{R}^{|\mathscr{A}|\times|\mathscr{R}|}$ is the link-route incidence matrix with entries $\delta_{a,r} = 1$ if link a is on route r and $\delta_{a,r} = 0$ otherwise.

Let W be a random variable representing the occurrence of different future scenarios; w and $\mathscr{W}$ are used to denote a realization of possible scenarios and the set of all realizations, respectively. Given a realization w, probabilistic link properties and OD demands can be determined as discussed in the previous section. Based on these parameters, the cost of traveling in the network (in terms of time for traveling) can be determined by a link flow-delay function $T_a: \mathbb{R} \to \mathbb{R}$, referred to herein as the cost function. For instance, the cost function recommended by the Bureau of Public Roads [29], referred to herein as BPR function, can be expressed as

$$T_a(f_a, w) = t_a^0(w)\cdot\left(1 + b_a\left(\frac{f_a}{C_a(w)}\right)^{n_a}\right) \tag{5}$$

where the free speed travel time t_a^0 and the link capacity C_a are associated with future scenarios and can be obtained according to Eqs. (1)–(3) [16]; f_a is the link flow on link a; and b_a and n_a are deterministic parameters of the cost function. It should be noted that using BPR function may run into issues when severe congestion is expected. More generalized cost functions are available to reflect uncertainties of link properties during or immediately after a short-term adverse event (e.g. traffic accidents and extreme weather conditions). For instance, Lam et al. [8] proposed a cost function that can reflect the effects of rainfall intensities on road conditions. Nevertheless, as mentioned previously, this study is focused on the long-term uncertainties where widespread severe congestion is not likely to be persistent for the time horizon of interest. Therefore, the potential numerical issues of using BPR function can be avoided.

Based on Eq. (4), the sum of all link costs, referred to as the travel cost function of a network, can be represented in terms of route flow $\mathbf{h}$ as follows:

$$\Phi(\mathbf{h}, w) = \Delta^{\mathrm{T}} T(\Delta\mathbf{h}, w) \tag{6}$$

where $T: \mathbb{R}^{|\mathscr{A}|} \to \mathbb{R}^{|\mathscr{A}|}$ is a vector of functions; each element of this vector is a cost function T_a associated with a link. Associated with a certain route flow pattern $\mathbf{h}$, $\mathbf{u} \in \mathbb{R}^{|\mathscr{C}|}$ is used to denote the shortest route cost between OD pairs. For OD demands $\mathbf{Q}(w) \in \mathbb{R}^{|\mathscr{C}|}$ with respect to scenario w, traffic assignment models seek to find a flow pattern that can satisfy the following relation:

$$\Gamma^{\mathrm{T}}\mathbf{h} = \mathbf{Q}(w) \tag{7}$$

where $\Gamma = (\gamma_{r,c}) \in \mathbb{R}^{|\mathscr{R}|\times|\mathscr{C}|}$ is the route-OD incidence matrix with entries $\gamma_{r,c} = 1$ if route r is connecting OD c and $\gamma_{r,c} = 0$ otherwise.

3.2. Robust traffic assignment using expected residual minimization approach

With the preceding symbols and notations, traffic assignment problems can be formulated based on Wardrop's first principle of user equilibrium as a nonlinear complementarity problem (NCP), that is, with $n = |\mathscr{R}| + |\mathscr{C}|$ and $\mathbf{x} = (\boldsymbol{h}, \boldsymbol{u})$, find an $\mathbf{x}^* \in \mathbb{R}^n$ such that [5]

$$G(\mathbf{x}^*, w)^{\mathrm{T}}\mathbf{x}^* = 0, \quad G(\mathbf{x}^*, w) \geqslant 0, \quad \mathbf{x}^* \geqslant 0 \tag{8}$$

where $\geqslant$ is the "succeed or equal to" sign indicating that all elements in a vector are greater than or equal to a certain value; $G: \mathbb{R}^n \to \mathbb{R}^n$ is expressed as

$$G(\mathbf{x}, w) = \begin{pmatrix} \Phi(\mathbf{h}, w) - \Gamma\mathbf{u} \\ \Gamma^{\mathrm{T}}\mathbf{h} - \mathbf{Q}(w) \end{pmatrix} \tag{9}$$

The NCP in Eq. (8) can be further expressed as a system of nonlinear equations, shown as follows [18]:

$$\min(\mathbf{x}, G(\boldsymbol{x}, w)) = 0 \tag{10}$$

where $\min(\mathbf{v}_1, \mathbf{v}_2)$, $\mathbf{v}_1, \mathbf{v}_2 \in \mathbb{R}^n$, is an element-wise operator that returns the minimum of the ith elements in $\mathbf{v}_1$ and $\mathbf{v}_2$ as its ith entry.

For each realization w of future scenarios, the solution of Eq. (10) is denoted as $\mathbf{x}_w$, and the set of all these solutions associated with all future scenarios is denoted as $\mathscr{S}_W$. It is worth mentioning that, for the BPR function, $\mathbf{x}_w$ is a unique solution with respect to each scenario. Nonetheless, $\mathscr{S}_W$ may not be singleton or convex. Robust traffic assignment models attempt to seek a flow pattern that satisfies the following condition:

$$\mathbf{x}_R = \underset{\mathbf{x}\in\mathbb{R}^n_+}{\operatorname{argmin}}\, \mathbb{E}[\operatorname{dist}(\mathbf{x}, \mathscr{S}_W)] \tag{11}$$

where $\operatorname{dist}(\mathbf{x}, \mathscr{S}_W)$ is the Euclidean distance from $\mathbf{x}$ to the elements in $\mathscr{S}_W$. This optimization problem is referred to herein as the crude model for robust traffic assignment. Directly solving Eq. (11) can be impractical as it requires the determination of traffic flow patterns with respect to all possible scenarios. Also, as shown subsequently, the solution may not be unique. Therefore, the ERM approach, first proposed

by Zhang et al. [18], is used herein. Instead of directly finding a robust flow pattern defined in Eq. (11), the ERM model considers residuals defined as follows:

$$r_w(\mathbf{x}) := ||\min(\mathbf{x}, G(\mathbf{x}, w))|| \tag{12}$$

where $||\cdot||$ is the Euclidean norm of vectors; and $r_w: \mathbb{R}^n \to \mathbb{R}_+$ is usually referred to as a residual of NCP($G(\mathbf{x}, w)$). The ERM approach for robust traffic assignment aims at determining a flow pattern that minimizes the expected value of all residuals associated with different future scenarios, represented mathematically as:

$$\mathbf{x}_{ERM} = \underset{\mathbf{x}\in\mathbb{R}_+^n}{\operatorname{argmin}} g(\mathbf{x}) := \mathbb{E}[||\min(\mathbf{x}, G(\mathbf{x}, w))||^2] \tag{13}$$

The existence of $\mathbf{x}_{ERM}$ has been proved by Zhang et al. [18]. Regarding the relation between $\mathbf{x}_R$ and $\mathbf{x}_{ERM}$, it has also been demonstrated that under some mild assumptions [18], the following relation holds:

$$\exists\, \eta \in \mathbb{R}_{++}, \text{ such that } \mathbb{E}[\operatorname{dist}(\mathbf{x}_{ERM}, \mathscr{S}_W)] \le \eta\sqrt{g(\mathbf{x}_{ERM})} = \eta\sqrt{\min_{\mathbf{x}\in\mathbb{R}_+^n} g(\mathbf{x})} \tag{14}$$

Eq. (14) indicates that $\mathbb{E}[\operatorname{dist}(\mathbf{x}_{ERM}, \mathscr{S}_W)]$ is likely to be small and, therefore, $\mathbf{x}_{ERM}$ can be treated as a robust solution against the uncertainties of future scenarios. Once $\mathbf{x}_{ERM}$ is obtained, it can be easily decomposed to the robust route flow pattern ($\mathbf{h}_{ERM}$) and the robust minimum travel cost between OD pairs ($\mathbf{u}_{ERM}$), both of which can be used in risk assessment.

4. Implementation of ERM approach for robust traffic assignment

In this section, a novel algorithm for implementing the ERM approach of robust traffic assignment is developed. This algorithm uses a smoothening method for the "min" operator in the definition of residuals [Eq. (12)] so that the nonsmooth optimization problem can be tackled sequentially by a series of subproblems with smooth objective functions. For each subproblem, quasi-Newton technique is used to find the solution. A sampling technique is also incorporated to the developed algorithm to efficiently evaluate objective functions of subproblems.

4.1. Smoothing method

It can be noticed that the "min" operator within the expectation operator in Eq. (13) leads to a nonsmooth objective function (a function with discontinuous first order partial derivatives) that cannot be easily handled. Therefore, a smoothing method is used herein. Specifically, the nonsmooth objective function $g(\cdot)$ in Eq. (13) is decomposed into a series of smoothing functions $g(\cdot,\mu)$ with monotonically increasing μ. The original optimization problem is then divided into a series of subproblems with smooth objectives functions $g(\cdot,\mu)$. The smoothing functions should satisfy the following requirements [18]:

$$\lim_{\mathbf{z}\to\mathbf{x},\mu\downarrow 0} g(\mathbf{z}, \mu) = g(\mathbf{x}) \tag{15}$$

$$\{\lim_{\mathbf{z}\to\mathbf{x},\mu\downarrow 0} \nabla_{\mathbf{x}} g(\mathbf{z}, \mu)\} \text{is nonempty and bounded} \tag{16}$$

In this paper, the following smoothing approximation for $\min(x_i, G_i(\mathbf{x}, w))$ is used [18]:

$$\phi(x_i, G_i(\mathbf{x}, w), \mu) = \begin{cases} G_i(\mathbf{x}, w) & \text{if} x_i - G_i(\mathbf{x}, w) \ge \mu/2 \\ x_i - \frac{1}{2\mu}\left(x_i - G_i(\mathbf{x}, w) + \frac{\mu}{2}\right)^2 & \text{if} -\mu/2 < x_i - G_i(\mathbf{x}, w) < \mu/2 \\ x_i & \text{if} x_i - G_i(\mathbf{x}, w) \le -\mu/2 \end{cases} \tag{17}$$

where $G_i(\mathbf{x}, w)$ is the i-th entry of vector $G(\mathbf{x}, w)$. The objective function in each subproblem can be expressed as

$$g(\mathbf{x}, \mu) = \mathbb{E}[H_w(\mathbf{x}, \mu)^{\mathrm{T}} H_w(\mathbf{x}, \mu)] \tag{18}$$

where $H_w: \mathbb{R}^n \times \mathbb{R}_{++} \to \mathbb{R}$ is given by

$$H_w(x, \mu) = \begin{pmatrix} \phi(x_1, G_1(\mathbf{x}, w), \mu) \\ \phi(x_2, G_2(\mathbf{x}, w), \mu) \\ \vdots \\ \phi(x_n, G_n(\mathbf{x}, w), \mu) \end{pmatrix} \tag{19}$$

The gradient of $g(\mathbf{x}, \mu)$ with respect to $\mathbf{x}$ can then be expressed as

$$\nabla_{\mathbf{x}} g(\mathbf{x}, \mu) = 2\mathbb{E}[\nabla_{\mathbf{x}} H_w(\mathbf{x}, \mu) H_w(\mathbf{x}, \mu)] \tag{20}$$

where $\nabla_{\mathbf{x}} H_w(\mathbf{x}, \mu) \in \mathbb{R}^{n\times n}$ is the gradient of $H_w(\mathbf{x}, \mu)$ with respect to $\mathbf{x}$ and can be determined as follows:

$$(\nabla_{\mathbf{x}} H_w(\mathbf{x}, \mu)^{\mathrm{T}})_i = \begin{cases} (\nabla_{\mathbf{x}} G(\mathbf{x}, w)^{\mathrm{T}})_i & \text{if} x_i - G_i(\mathbf{x}, w) \ge \mu/2 \\ I_i - (I_i - (\nabla_{\mathbf{x}} G(\mathbf{x}, w)^{\mathrm{T}})_i)\left(\frac{x_i - G_i(\mathbf{x}, w)}{\mu} + \frac{1}{2}\right) & \text{if} -\mu/2 < x_i - G_i(\mathbf{x}, w) < \mu/2 \\ I_i & \text{if} x_i - G_i(\mathbf{x}, w) \le -\mu/2 \end{cases} \tag{21}$$

in which $(\nabla_{\mathbf{x}} H_w(\mathbf{x}, \mu)^{\mathrm{T}})_i$ is the i-th row of the transpose of $\nabla_{\mathbf{x}} H_w(\mathbf{x}, \mu)$; I_i is a row vector, in which the i-th entry is equal to one while the others are equal to zero. Algorithmically, the proposed smoothing method can be implemented as follows.

Algorithm 1.1 (*Smoothing*). Let $\mu_0 > 0$ and $0 < \gamma < 1$. Let $\mathbf{x}_0 \in \mathbb{R}_+^n$ be an initial guess of $\mathbf{x}$.***for k*** ≥ 0:

1. Solve the following subproblem of optimization:

$$\min_{\mathbf{x}\in\mathbb{R}_+^n} g(\mathbf{x}, \mu) := \mathbb{E}[H_w(\mathbf{x}, \mu)^{\mathrm{T}} H_w(\mathbf{x}, \mu)] \tag{22}$$

with an initial guess at $\mathbf{x}_k$, and set $\mathbf{x}_{k+1} = \underset{\mathbf{x}\in\mathbb{R}_+^n}{\operatorname{argmin}} g(\mathbf{x}, \mu)$;

2. Set $\mu_{k+1} = \gamma\mu_k$.

4.2. Properties of subproblem

The existence of the original optimization problem in Eq. (13) has been proved by Zhang et al. [18]. Therefore, based on the properties of the smoothing function [i.e. Eqs. (15) and (16)], the solution for subproblem [Eq. (22)] should also exist, at least for small μ. It is shown herein that the objective function as specified by Eq. (22) is generally nonconvex and nonunique, but the (local) minimizer of Eq. (22) is isolated given the BPR function in Eq. (5).

For the purpose of illustration, consider a minimalistic network composed of two nodes and one link connecting them. Based on the previous notations, the following properties of this network can be easily obtained:

$$h = f \in \mathbb{R}_+ \tag{23}$$

$$\Phi(h, w) = T(f, w) \tag{24}$$

$$\mathbf{x} = (h, u)^{\mathrm{T}} \in \mathbb{R}_+^2 \tag{25}$$

$$G(\mathbf{x}, w) = \begin{pmatrix} \Phi(h, w) - u \\ h - Q(w) \end{pmatrix} \in \mathbb{R}^2 \tag{26}$$

Without losing any generality, only cases where W is a discrete random variable representing a finite number of future scenarios.

Using the network with only one link, the following two examples are first considered:

Example 1. Consider first the deterministic minimalistic network with

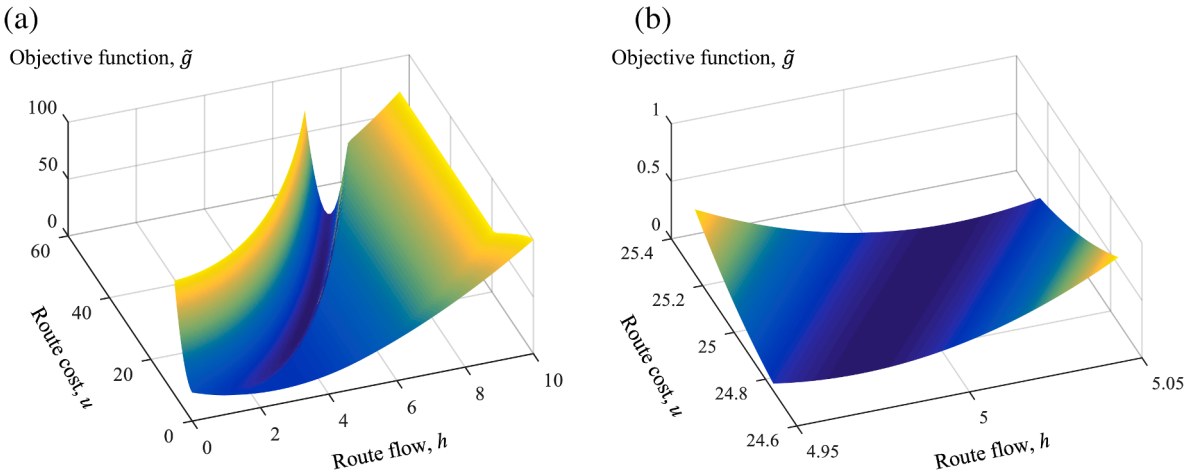

Fig. 3. Nonconvex objective function of subproblem.

$T(\mathbf{x}) = h^2$, $Q = 5$ and $\mu = 1$.

Example 2. For the same network in Example 1, Add a nonlinear time-related component to the link cost function. The link cost function can thus be expressed as

$$T(\mathbf{x}) = h^2 + \frac{u^2}{125} \tag{27}$$

For Example 1, Fig. 3(a) presents the objective function surface with $g(\mathbf{x}, \mu) \leq 100$. It can be easily observed that the objective function is not a convex function. In Example 2, the objective function is presented in Fig. 4. It can be determined that there exist two solutions, i.e. $x^{*,1} = (5, 34.56)^{\mathrm{T}}$ and $x^{*,2} = (5, 90.45)^{\mathrm{T}}$ that can minimize the objective function in Eq. (22). Based on the above observations, the following remark is made:

Remark 1. Generally, the objective function of subproblem Eq. (22) is nonconvex, and the optimization solution is not unique.

Despite the general case of nonconvexity, the form of the BPR cost function indicates that the second order sufficiency condition of optimality is likely to be satisfied. In fact, since the only (inequality) constraint (i.e. nonnegativity of $\mathbf{x}$) is an affine function and the objective function is continuous and twice differentiable, the optimality is defined by the Karush-Kuhn-Tucker (KKT) conditions with linearity constraint qualification (LCQ) (Boyd & Vandenberghe 2009). The second order sufficiency condition indicates that, given the BPR cost function, the local minimizer of Eq. (22) is isolated. The property of isolated local minima indicates that the solution is unique in a small region near the optimum. This feature can be observed in the objective surface of Example 1 near the minimum value, as shown in Fig. 3(b). Therefore, if the optimization subproblem is started somewhere near a local optimum, it is likely to obtain the optimum using convex optimization methods.

Finally, the ERM model is compared with the crude model in Eq. (11) using the follow example.

Example 3. Consider the network in Example 1 with uncertain traffic demand: the probability of $Q = 4$ is 0.5; the probability of $Q = 5$ is 0.5.

The contour of the objective function, the solution using ERM model, and the solutions of deterministic traffic assignment associated with each individual value of Q are shown in Fig. 5. Furthermore, the solutions satisfying the robustness condition in Eq. (11) are also denoted. It can be seen that all points on the line connecting the two solutions for $Q = 4$ and $Q = 5$ are solutions for Eq. (11). It is impossible to obtain a specific traffic pattern solely using Eq. (11). Therefore, the following remark can be stated.

Remark 3. The crude model for robust traffic assignment [Eq. (11)] may have non-isolated solutions that cannot be easily utilized for risk

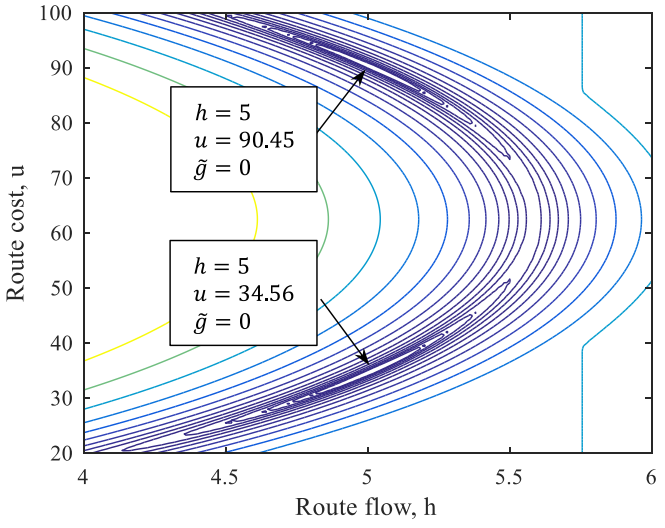

Fig. 4. Subproblem with two solutions.

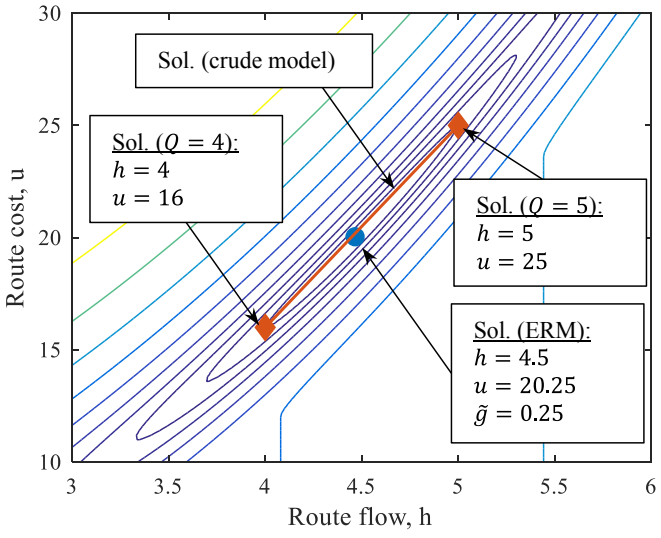

Fig. 5. ERM model vs. crude model for robust traffic assignment.

assessment; the ERM model, on the other hand, can provide isolated solutions satisfying the definition of robustness.

4.3. Solution of subproblem

Based on the preceding discussions, the ERM model for robust traffic assignment reduces to a series of optimization subproblems. In the original proposal of the ERM model, Zhang et al. [18] adopted the rudimentary steepest descent method to solve subproblems. As demonstrated later in the example, the steepest descent method does not have a satisfactory convergence rate. In fact, the poor performance of the simple steepest descent method can be anticipated by observing the shape of the objective function as that shown in Fig. 3(b). This shape implies that there will be many zigzags in searching directions when the steepest descent method is used. In this paper, limited-memory Broyden-Fletcher-Goldfarb-Shanno (L-BFGS) algorithm is employed due to its computational efficiency and numerical robustness even in nonconvex problems [30]. The nonnegative constraint of $\mathbf{x}$ can be easily implemented using the Euclidean projection:

$$[\mathbf{x}]_+ = (x_i, \text{ if } x_i \geq 0; \ 0, \text{ otherwise}) \tag{28}$$

For the implementation of L-BFGS, the gradient and Hessian of the objective function are first deduced. It is denoted that the discrete random variable W has ω mutually exclusive and collectively exhaustive states. Therefore, the objective function in Eq. (22) can be rewritten as

$$g(\mathbf{x}, \mu) = \mathbb{E}[H_w(\mathbf{x}, \mu)^{\mathrm{T}} H_w(\mathbf{x}, \mu)] = \sum_{i=1}^{\omega} p_i \cdot (H_{w_i}(\mathbf{x}, \mu)^{\mathrm{T}} H_{w_i}(\mathbf{x}, \mu)) \tag{29}$$

where p_i is the probability of $\{E: W = w_i\}$, i.e. $0 \leq p_i \leq 1$ and $\sum_i^{\omega} p_i = 1$. The gradient of $g(\mathbf{x}, \mu)$ with respect to $\mathbf{x}$ can then be expressed as [30]

$$\begin{aligned} \nabla_{\mathbf{x}} g(\mathbf{x}, \mu) &= 2 \sum_{i=1}^{\omega} p_i \cdot (\nabla_{\mathbf{x}} H_{w_i}(\mathbf{x}, \mu) H_{w_i}(\mathbf{x}, \mu)) \\ &= 2 \sum_{i=1}^{\omega} p_i \cdot \sum_{j=1}^{n} \phi_i(x_j, G_j(\mathbf{x}, w_i), \mu) \cdot \nabla_{\mathbf{x}} \phi_i(x_j, G_j(\mathbf{x}, w_i), \mu) \end{aligned} \tag{30}$$

where $\phi_i: \mathbb{R}_+ \times \mathbb{R}^n \times \mathbb{R}_{++} \to \mathbb{R}$ is the smoothing function [Eq. (17)] with respect to $\{E: W = w_i\}$.

Based on the expression of the gradient given in Eq. (30), the L-BFGS algorithm can be summarized as follows [30].

Algorithm 1.2 (*L-BFGS*). Let $m \in \mathbb{Z}_{++}$ be the number of steps memorized for the inverse Hessian approximation and $\mathbf{y}_0 = \mathbf{x}_k$ from Algorithm 1.1; denote $f(\mathbf{x}) = g(\mathbf{x}, \mu_k)$, $\mathbf{s}_t = \mathbf{y}_{t+1} - \mathbf{y}_t$, and $\mathbf{z}_t = \nabla f(\mathbf{y}_{t+1}) - \nabla f(\mathbf{y}_{t+1})$.***for*** $j \geqslant 0$:

1. Choose an initial guess of inverse Hessian $\boldsymbol{H}_j^0$;
2. Compute direction $\mathbf{p}_j = -\mathbf{H}_j \nabla f(\mathbf{y}_j)$ using the following steps:
   a. $\boldsymbol{q} = \nabla f(\boldsymbol{y}_j)$;
   b. ***for*** $i = j-1, \ j-2, \ \ldots, \ j-m$:
      $\rho_i = 1/(\boldsymbol{z}_i^{\mathrm{T}} \boldsymbol{s}_i)$; $\alpha_i = \rho_i \boldsymbol{s}_i^{\mathrm{T}} \boldsymbol{q}$; $\boldsymbol{q} = \boldsymbol{q} - \alpha_i \boldsymbol{y}_i$;
   c. $\boldsymbol{r} = \boldsymbol{H}_j^0 \boldsymbol{q}$;
   d. ***for*** $i = j-m, j-m+1, \ldots, j-1$:
      $\rho_i = 1/(\boldsymbol{z}_i^{\mathrm{T}} \boldsymbol{s}_i)$; $\beta = \rho_i \boldsymbol{y}_i^{\mathrm{T}} \boldsymbol{r}$; $\boldsymbol{r} = \boldsymbol{r} + (\alpha_i - \beta)\boldsymbol{s}_i$;
   e. stop with result $\boldsymbol{H}_j \nabla f(\boldsymbol{y}_j) = \boldsymbol{r}$;
3. Compute $\boldsymbol{y}_{j+1} = [\boldsymbol{y}_j + \alpha_j \boldsymbol{p}_j]_+$, where α_j should satisfy the Wolfe conditions;
4. ***if*** $j > m$: discard the vector pair $\{\boldsymbol{s}_{j-m}, \boldsymbol{z}_{j-m}\}$ from storage;
5. Compute and save $\boldsymbol{s}_j = \boldsymbol{y}_{j+1} - \boldsymbol{y}_j$, $\boldsymbol{z}_j = \nabla f(\boldsymbol{y}_{j+1}) - \nabla f(\boldsymbol{y}_{j+1})$;
6. $j = j+1$ and go back to step 1 until convergence, $\boldsymbol{x}_{k+1} = \boldsymbol{y}_j$.

Compared with other methods, the main advantages of L-BFGS are as follows. First, the algorithm only requires the storage of initial inverse Hessian $\mathbf{H}_j^0$ that can be sparse. Therefore, it is especially attractive to large scale problems where storing Hessians is computationally prohibitive. Secondly, for cases where enumeration of all future scenarios as well as their occurrence probabilities is impractical, Monte Carlo simulation instead of Eq. (30) is needed for the evaluation of objective functions. L-BFGS used herein is applicable for these cases since the recursive procedure in step 2 serves as an implicit filtering process of Hessian approximation. Therefore, the numerical noise from Monte Carlo simulation can be reduced so that the numerical robustness of the algorithm is improved. The number of memorized steps (m) can affect the computational efficiency and numerical robustness, with higher efficiency and lower robustness associated with lower m. A pragmatic range, from $m = 3$ to $m = 20$, has been recommended [30]. In cases where Monte Carlo simulation is used for objective evaluation, m should be related to the number of samples, i.e. a larger number of samples may imply a lower m and vice versa.

4.4. Efficient sampling for evaluation of the objective function

As stated previously, the objective functions of subproblems may require Monte Carlo simulation for evaluation. An efficient sampling scheme can reduce the number of samples for converged estimation. This means that efficient sampling is not only beneficial to computational efficiency but also critical to numerical robustness as less severe fluctuation can be expected. To this end, Latin hypercube sampling (LHS) is used to evaluate Eq. (22). In order to control the correlation between random variables, simulated annealing (SA) is adopted to permute LHS samples so that specified correlation can be achieved [31]. The algorithm for LHS with correlation control using SA is summarized as follows.

Algorithm 1.3 (*SA-LHS*). Let $T_0 > 0$ be an analogous initial temperature for simulated annealing, $\mathbf{u}_0$ be an initial arrangement of LHS samples, and T_c with $0 < T_c < T_0$ be the cold temperature indicating the termination of SA. RandomPermute is an operator that permutes the arrangement of LHS samples randomly; CorrelationNorm is the norm of the correlation matrix of samples; CoolDown is an operator that reduce the temperature in each step.***for*** $t \geq 0$ ***and*** $T_t > T_0$ ***and*** target correlation has not been reached**:**

1. Generate a set of random successors of $\mathbf{u}_t$: $\{\mathbf{U}_{t+1}\} = \text{RandomPermute}(\mathbf{u}_t)$;
2. ***for*** $\mathbf{u}_{t+1}$ ***in*** $\{\mathbf{U}_{t+1}\}$:

   $\Delta E = \text{CorrelationNorm}(\mathbf{u}_t) - \text{CorrelationNorm}(\mathbf{u}_{t+1})$

   if $\Delta E > 0$:Accept $\mathbf{u}_{t+1}$ and exit *for*-loop;***else***:Accept $\mathbf{u}_{t+1}$ with probability of $\exp(-\Delta E/T_t)$;If accepted, then exit *for*-loop;Otherwise continue with the next $\mathbf{u}_{t+1}$ in $\{\mathbf{U}_{t+1}\}$;

3. Update $\mathbf{u}_t$ with $\mathbf{u}_{t+1}$, $T_{t+1} = \text{CoolDown}(T_t)$ and $t = t+1$.

5. Societal risk assessment of transportation networks

In general, failure risk of infrastructure with respect to multiple hazards can be defined as [32]

$$R_H = \sum_{S \in \cup H_i} P[F|S] \cdot P[S] \cdot C \tag{31}$$

where R_H is the failure risk of infrastructure; $\cup H_i$ is the set of mutually exclusive and collectively exhaustive events where at least one hazard occurs; S is one event in $\cup H_i$; C is the consequence in monetary value. Risk defined in Eq. (31) can also be interpreted as the expected value of consequences considering multiple hazards [33]. In this section, it is shown how the results of robust traffic assignment can be used to estimate societal risk of transportation networks under uncertainties due to climate change and population growth.

For transportation networks, societal consequences at a future point-in-time (t) can be converted to monetary terms from total travel time (TTT) and total travel distance (TTD) defined as [32]:

$$C_{time}(t) = [c_{AW} O_{car} \bullet (1 - \alpha) + (c_{ATC} O_{truck} + c_{good}) \bullet \alpha] \cdot \frac{T_{travel}}{(1 + r)^t} \tag{32}$$

$$C_{run}(t) = [c_{run,car} \bullet (1 - \alpha) + c_{run,truck} \bullet \alpha] \cdot \frac{D_{travel}}{(1 + r)^t} \tag{33}$$

$$C_{net}(t) = C_{time}(t) + C_{run}(t) \tag{34}$$

where c_{AW} is the average wage of car drivers; O_{car} is the average vehicle occupancies for cars; α is the ratio of average daily truck traffic to average daily traffic; c_{ATC} is the average compensation for truck drivers; O_{truck} is the average vehicle occupancies for trucks; c_{good} is the time value of cargo; $c_{run,car}$ is the running cost of cars; $c_{run,truck}$ is the running cost of trucks; r is the discount rate of money; and T_{travel} and D_{travel} are the TTT and TTD, defined respectively as follows [17]:

$$T_{travel} = \text{sum}(\mathbf{f} \circ \text{T}(\mathbf{f})) \tag{35}$$

$$D_{travel} = \text{sum}(\mathbf{f} \circ \mathbf{L}) \tag{36}$$

where $\text{sum}(\cdot)$ is the summation operator to all vector elements; $\circ$ is the Hadamard product operator for element-wise multiplication; $\mathbf{L} \in \mathbb{R}^{|\mathscr{A}|}$ is the vector of link lengths. For the ease of the following discussion, the following notations are used:

$$k_1 = \frac{c_{AW} O_{car} \bullet (1 - \alpha) + (c_{ATC} O_{truck} + c_{good}) \bullet \alpha}{(1 + r)^t} \tag{37}$$

$$k_2 = \frac{c_{run,car} \bullet (1 - \alpha) + c_{run,truck} \bullet \alpha}{(1 + r)^t} \tag{38}$$

Based on the definition of risk (i.e. expected consequences), societal risk of a transportation network under uncertainties due to climate change and population growth can be expressed as

$$R_H = k_1 \cdot \mathbb{E}[\text{sum}(\mathbf{f} \circ \text{T}(\mathbf{f}))] + k_2 \cdot \mathbb{E}[\text{sum}(\mathbf{f} \circ \mathbf{L})] \tag{39}$$

where $\mathbf{f}$ is a random vector depending on the realization of future scenarios and the network supply and demand associated with the scenario. In general, societal risk defined in Eq. (39) is evaluated using Monte Carlo simulation. It should be noted that this Monte Carlo simulation is different from that for objective evaluation in the proposed method. Specifically, for each sample within in the simulation, deterministic traffic assignment, which itself is an optimization problem, must be conducted. Therefore, direct Monte Carlo simulation for societal risk assessment may easily become infeasible for larger transportation networks. By contrast, Monte Carlo simulation for objective function evaluation in robust traffic assignment [Eq. (22)] needs only to compute an analytical expression.

In the proposed method, the traffic flow pattern from robust traffic assignment (referred to herein as robust flow pattern) is used to estimate the societal risk in Eq. (39). Based on Eq. (14), the robust flow pattern is a flow pattern that is close to all flow patterns under all realizations of supplies and demands (i.e. realizations of $\mathbf{f}$). According to Eq. (9), its corresponding OD costs can be expressed as $\Gamma \mathbf{u}_R$, where $\mathbf{x}_{ERM} = \{\mathbf{h}_R^T, \mathbf{u}_R^T\}^T$. Therefore, the following equation can be used to approximate societal risk:

$$\widehat{R}_H = k_1 \cdot \text{sum}(\mathbf{h}_R \circ (\Gamma \mathbf{u}_R)) + k_2 \cdot \text{sum}((\Gamma^{\text{T}} \mathbf{h}_R) \circ \mathbf{L}_R) \tag{40}$$

where $\mathbf{h}_R$ and $\mathbf{u}_R$ is the robust route flow vector and the robust OD cost vector, respectively; $\mathbf{L}_R$ is the robust link length that can be approximated as (a) original link length $\mathbf{L}$ (best scenario), (b) longest link length $\mathbf{L}_w$ (worst scenario), or (c) a robust pattern bounded by $\mathbf{L}$ and $\mathbf{L}_w$. If detours are generally available and short (e.g. in urban transportation networks), original link length $\mathbf{L}$ can provide sufficiently accurate results. Eq. (14) implies that the error produced by Eq. (40) compared to Eq. (39) is likely to be small. It can be seen that Eq. (40) converts Eq. (39) to a deterministic expression. Therefore, Monte Carlo simulation for risk assessment is no longer needed.

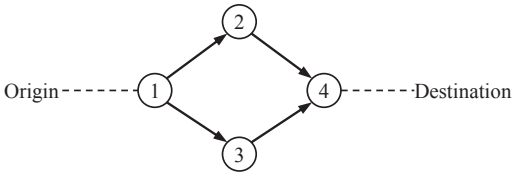

Fig. 6. Simple network model.

6. Illustrative examples

In this section, a simple network with 4 nodes, 4 links, 1 OD pair and 2 bridges is first analyzed to demonstrate the computational efficiency of the proposed method. To illustrate the application of the proposed method, a real-world highway bridge network in Camden County, New Jersey, is also analyzed for its life-cycle societal risk under uncertainties due to climate change and population growth. The effects of climate change and population growth are studied based on the obtained robust traffic flow pattern.

6.1. Demonstration of computational efficiency

A simple network is first considered to demonstrate the computational merits of the proposed method. The network has 4 nodes, 4 links and 1 OD pair, as shown in Fig. 6 [27]. The travel demand from origin 1 to destination 4 is 1000 vehicles/hour. The link cost function uses the BPR form [Eq. (5)] with $b_a = 0.1$ and $n_a = 4$. All four links of the network are assumed to have the same length $s_a = 20$km, free speed $v_a = 80$km/h, and practical capacity $C_a = 200$vehicles/hour. Two bridges are located on links 1–2 and 1–3. It is assumed that the detour lengths for bridges 1 and 2 are 5 km and 10 km, respectively, and the capacity drop due to bridge failures on both links is 50%. Due to the stochastic bridge conditions, the link properties of the network are subjected to uncertainties. Robust traffic assignment is used to obtain the robust flow pattern under these uncertainties. The design variables of the optimization problem are $\mathbf{x} = \{h_1, h_2, u\}$ where h_1 and h_2 are the route flows on routes 1–2–4 and 1–3–4, respectively; and u is the travel cost from origin 1 to destination 4 (OD cost). The solution of the optimization subproblem is denoted as $\mathbf{x}^*$. As each bridge has two states (safe or failed), there are in total 4 possible network configurations. The objective function can be evaluated using Eq. (29) with $\omega = 4$. The values of each network configurations can be calculated as

$$\begin{cases} p_1 = \gamma \cdot \sqrt{p_x p_y (1 - p_x)(1 - p_y)} + p_x p_y & \text{both bridges fail} \\ p_2 = p_x - p_1 \geq 0 & \text{only bridge 1 fails} \\ p_3 = P_y - P_1 \geq 0 & \text{only bridge 2 fails} \\ p_4 = 1 - p_1 - p_2 - p_3 \geq 0 & \text{otherwise} \end{cases} \tag{41}$$

where p_x and p_y are the marginalized failure probabilities of bridges 1 and 2, respectively; γ is the coefficient of correlation of bridges failures.

6.1.1. Projected gradient vs. L-BFGS

As described previously, the proposed method uses L-BFGS as opposed to the projected gradient (PG) algorithm used by Zhang et al. [18]. It is shown through this example that the L-BFGS algorithm is more efficient than the PG algorithm. It is assumed herein that the failure probabilities of bridges 1 and 2 are 0.05 and 0.1, respectively, and the coefficient of correlation between failures of both bridges is 0.5. In order to visualize the comparison, the OD cost is fixed so that route flow h_1 and h_2 can be plotted against the value of the objective function. It can be considered that the current optimization is conducted in a slice of the original design variable space. This fixed OD cost is selected from the solution $\mathbf{x}^*$ of robust traffic assignment. Fig. 7 shows the last few steps before convergence using PG and L-BFGS algorithms for one of the subproblems with $\mu = 1.0$. It can be observed that the PG algorithm needs far more steps to convergence due to the zigzags while

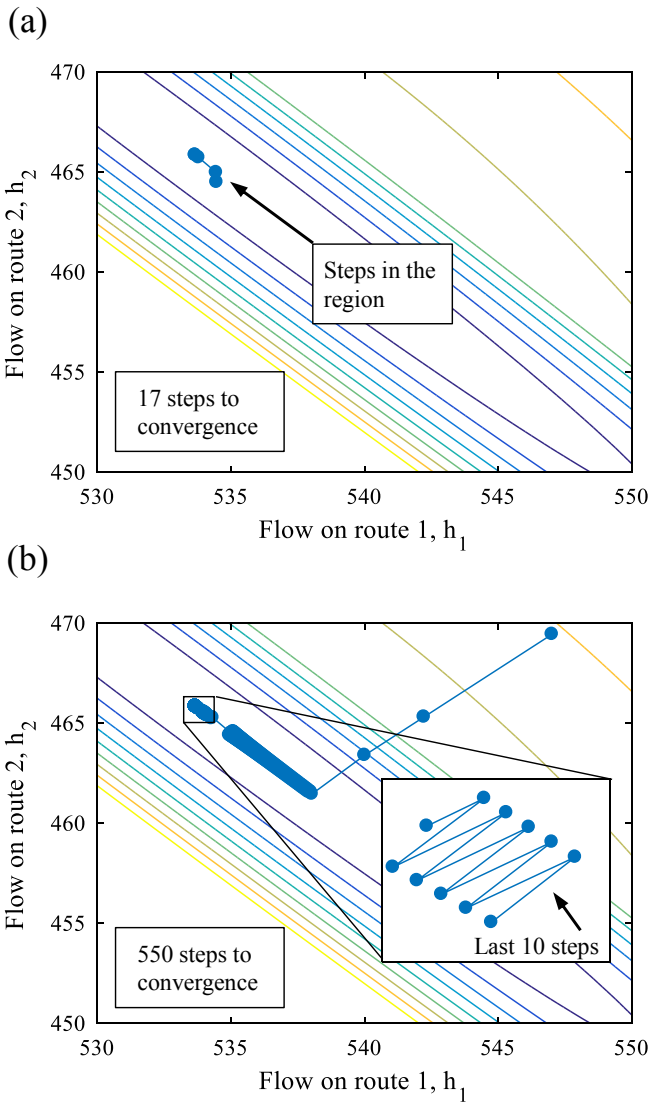

Fig. 7. Comparison of iteration steps using L-BFGS and PG algorithms: (a) L-BFGS algorithm; and (b) PG algorithm.

approaching the solution. On the other hand, the L-BFGS algorithm can achieve convergence in merely 17 steps. The comparison in Fig. 7 can very well demonstrate the efficiency of the proposed method in conducting robust traffic assignment.

6.1.2. Advantage of using Latin hypercube sampling

Another novelty of the proposed method is the use of LHS for the expectation operator in Eq. (22). In order to use LHS in the example, the Bernoulli random variables used to represent bridge conditions are first transformed to uniform random variables in the range [0, 1]. For a bridge with failure probability p, the event of bridge failure can be represented using the following equivalence [34]:

$$\{E: B = 1\} \Leftrightarrow \{E: U < p\} \tag{42}$$

where B is the Bernoulli random variable representing the bridge condition with parameter p, namely, $\{E: B = 1\}$ represents bridge failure and $\Pr[B = 1] = p$; U is a uniformly distributed random variable in the range of [0, 1]. With the transformation in Eq. (42), the expected value in Eq. (22) can either be estimated with uniform distribution samples from U using crude Monte Carlo simulation or LHS. Again, it is assumed herein that the coefficient of correlation between the performance functions defining failure of both bridges is 0.5. The comparison

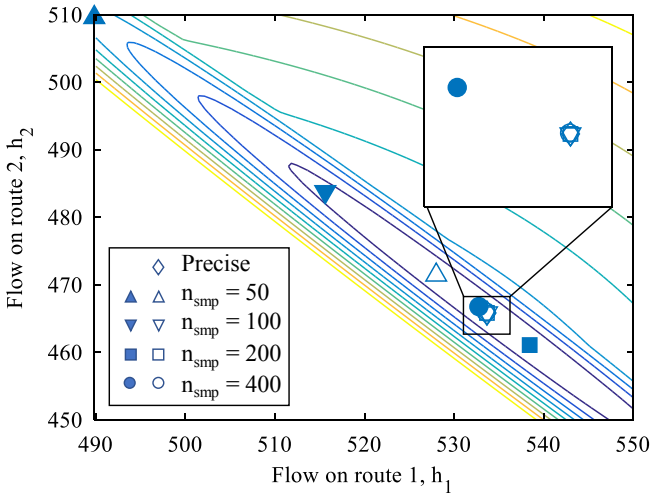

Fig. 8. Comparison of optimization solutions using crude Monte Carlo simulation (represented by the solid points) and LHS (represented by the hollow points).

between crude Monte Carlo simulation and LHS is conducted for the same subproblem with $\mu = 1.0$. The precise solution was already obtained from the previous comparison between L-BFGS and PG algorithms. Compared to this precise solution, the obtained solutions associated with different numbers of samples are shown in Fig. 8 for crude Monte Carlo simulation and LHS, respectively. It can be seen that crude Monte Carlo simulation needs much more samples (more than 400 samples) in order to converge to the precise solution. By contrast, LHS needs only 100 samples to reach convergence. Therefore, it is demonstrated that LHS can significantly reduce the number of samples when Monte Carlo simulation is needed for the evaluation of the objective function (Eq. (22)).

6.2. Societal risk assessment of bridge network

6.2.1. Network model and traffic demand

To illustrate the proposed method, societal risk of a real-world transportation network under uncertainties due to climate change and population growth is analyzed. Effects of climate change on structural deterioration and flood frequencies are taken into account; traffic demand between OD pairs increases as a result of population growth. The area under consideration is located in Camden County, New Jersey. The highway transportation network is modeled in this region. The network is shown in Fig. 9. In this network, highway intersections are modeled as network nodes, while highways are modeled as network links. According to the census data [35], a majority of Camden residents works in Philadelphia, Pennsylvania. Therefore, the traffic assignment model attempts to assign traffic demand for daily commute from Camden County to Philadelphia. The latter is represented by Node 1 located at the city center of Philadelphia. The traffic demands from Camden to Philadelphia are determined from 2010 census data [35], as summarized in Table 1. It should be noted that the average daily traffic data in the census database are converted to the hourly data in Table 1 by assuming a two-hour morning peak traffic period (“morning rush hours”). It is also assumed that each year has 260 working days.

For the network in Fig. 9, link costs are expressed using the general BPR form in Eq. (5) where $k = 0.15$. Link lengths in Eq. (5) can be determined from the geographic information system (GIS) model of the network. Link capacities are determined based on the number of lanes on each highway link. Each lane is estimated to have a capacity for 2000 vehicles/hour [15]. Free speed on highway links is assumed to be 90 km/h. Detailed information of network link properties is presented in Table 2. The region under consideration covers the majority of flood-

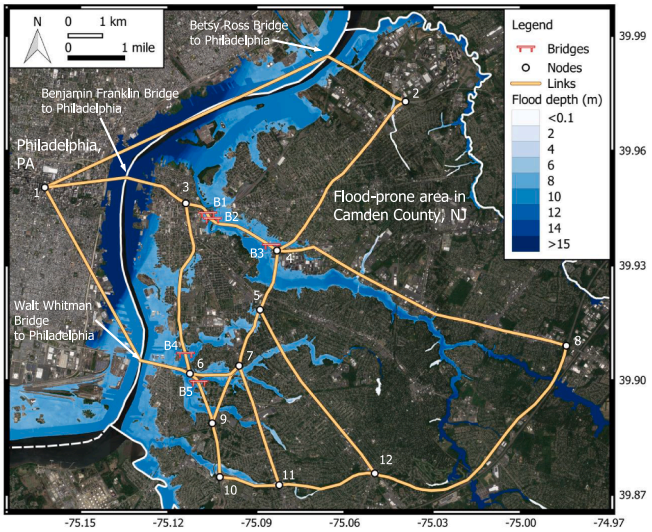

	Bridges under consideration				
	B1	B2	B3	B4	B5
NBI ID	406159	406158	406154	418154	418162
Flood depth (m)	2.58	3.20	2.72	3.18	3.25

Fig. 9. Highway transportation network, bridges under consideration, flood inundation depth in the region of interest.

Table 1
Average commute demand from Camden to Philadelphia.

Origin node	Demand (vehicles/hour)
2	890.2
3	100.2
4	878.2
5	505.6
6	89.2
7	173.8
8	1836.8
9	176.3
10	148.5
11	859.9
12	2083.0

Table 2
Link properties of the Camden-Philadelphia network.

Node A	Node B	Length (km)	Free speed (km/h)	Capacity (vehicles/hour)
1	2	11.68436	90	6000
1	3	4.310753	90	6000
1	6	7.237491	90	6000
3	6	5.116034	90	6000
3	4	3.095372	90	8000
2	4	5.806078	90	8000
4	5	1.817346	90	4000
4	8	9.050112	90	4000
5	7	1.756292	90	4000
7	9	1.859306	90	4000
6	9	1.615216	90	8000
9	10	1.585803	90	8000
7	11	3.658269	90	2000
5	12	5.832778	90	4000
10	11	1.772093	90	6000
11	12	2.891924	90	6000
12	8	7.764061	90	6000
6	7	1.535502	90	4000

prone lands in Camden County and includes around 80% of the total traffic demand from Camden County to Philadelphia. Therefore, it is believed that the current model is sufficient to realistically represent the highway usage in Camden County.

6.2.2. Hazard analysis

6.2.2.1. Hazard identification. Although both pavements and bridges can be analyzed with the proposed method, this example is focused on highway bridges under deterioration and floods. The hazard analysis herein aims to investigating the vulnerability of bridges subjected to two hazards: traffic and flood hazards. For traffic hazards, structural deterioration can compromise structural safety under traffic loads. It is considered that the occurrence rate of traffic load from the annually heaviest vehicle is 1 per year [36]. For flood hazards, dislodgement of bridge deck due to floods is considered as flood damage to bridges [37]. Other flood-related damage such as bridge scour, even though it is possible to be incorporated into the proposed method, is not investigated herein. Structural resistance to withstand the flood-induced uplifting load includes the self-weight of bridge superstructure and the connections (if existing) between super- and substructure. In this example, it is assumed that the self-weight of superstructure contributes primarily to the resistance to dislodgement. Therefore, structural deterioration is irrelevant to flood hazards.

6.2.2.2. Flood hazard. Located in an alluvial plain, Camden's flat geomorphology and low-lying position make it especially vulnerable to flood hazards, especially near the Delaware river where the lowest altitude is at the sea level. Based on the national hydrography database [38], the map of flood inundation depth associated with a 100-year flood is shown in Fig. 9. Five bridges in the region of interest are indicated in Fig. 9, together with their national bridge inventory (NBI) IDs and flood inundation depths. Table 3 presents further details of these five bridges under consideration.

From the structural demand side, bridge deck dislodgement under flood is related to flood conditions such as flood inundation depth and flow velocity [37]. In general, two approaches can be used to establish fragility curves of bridges: (a) structural reliability analysis; and (b) evidence-based survey from past extreme events. For reliability analysis approach, the load-carrying capacity of a bridge superstructure to withstand hydraulic uplifting force include its self-weight and the strength of super-to-substructure connections such as dowels, shear keys, vertical tie-downs, and restrainers [39,40]. On the loading side, a quasi-static hydraulic force associated with floods can be determined based on the design specifications [41,42]. By considering the uncertainties involved in both structural capacity and loading effects, reliability associated with deck dislodgement can be estimated with traditional reliability analysis methods such as first order reliability method (FORM). It should be noted that this approach requires the detailed knowledge of bridges and on-site flow conditions. This information is usually difficult to obtain for analysis at the regional level

Table 3
Bridges under consideration in the Camden-Philadelphia network.

Bridge ID	Link	Year (re) built	Deck condition	Inundation depth (m)	Detour (km)	Capacity drop (%)
406,154	3–4	1994	6	2.719688	6	0.9
418,154	3–6	1954	5	3.180754	4	0.5
406,158	3–4	1998	4	3.203932	6	0.9
406,159	3–4	1972	6	2.577504	6	0.9
418,162	6–9	1956	6	3.250323	0.2	0.5

where complete information on all bridges is most of the time not accessible. As a result, regional risk assessment usually adopts simple fragility curves obtained using the second approach [43,44]. This evidence-based approach is also utilized in this example. In this paper, failure probabilities associated with deck dislodgment is assumed to be related to the flood inundation depth. The fragility curve with respect to inundation depth is obtained based on the bridge damage data in a similar event. In particular, results in Shoji & Moriyama [45] are used to establish the following relation between failure probabilities and flood inundation depths:

$$P_{f,FLD}(d_{FLD}) = -0.006119 \cdot d_{FLD}^2 + 0.1387 \cdot d_{FLD} - 0.09707 \quad (43)$$

where $P_{f,FLD}$ is the failure probability of bridges under flood hazards; and d_{FLD} is the flood inundation depth (m).

6.2.2.3. Traffic hazard. Bridges deteriorate due to aggressive environmental stressors. Structural deterioration can reduce the load-carrying capacities of bridges and jeopardize structural safety under traffic loads. Vulnerability of deteriorating bridges to traffic hazards can be directly represented by the decreasing structural reliability throughout the service life of bridges. In this example, a linear deterioration model in terms of reliability index is used to model structural deterioration [46].

The five bridges under consideration were all built in the last century and have been in service for a relatively long time. To better represent their current conditions, the current reliability indices of the bridges are determined based on the condition ratings of decks following the approach in Yang & Frangopol [27]. Specifically, the reliability index with respect to a condition rating can be determined as

$$\beta_0(X) = \frac{0.64 \cdot (X - 2)}{\sqrt{(0.64X - 0.28)^2 \cdot \delta_R^2 + \delta_S^2}} \quad (44)$$

where X is the condition rating of bridge deck ($2 \le X \le 8$); $\beta_0(X)$ is the reliability index associated with condition rating X; and $\delta_R = 0.15$ and $\delta_S = 0.375$ are coefficients of variation of resistance and loading effects, respectively. It is also assumed that the deterioration initiation time is zero considering the long service time of the five bridges. Therefore, the linear deterioration model in Frangopol et al. [46] can be simplified as

$$\beta(t) = \beta_0(X) - \alpha \cdot t \quad (45)$$

where α is the deterioration rate.

6.2.3. Identification of future scenarios

As mentioned previously, climate change can affect both structural deterioration and extreme hydrologic events. In this example, two climate change scenarios are considered, namely, mild change and severe change. The mild change scenario is characterized by a smaller deterioration rate and a slower increase in the frequency of extreme floods. Specifically, the deterioration rate α is assumed to be 0.02 per year; the annual occurrence probability of a 100-year flood is assumed to increase linearly with respect to time from 0.01 to 0.02 after 100 years. For severe change, the deterioration rate is assumed to be 0.04, and the annual occurrence probability of a 100-year flood is assumed to increase linearly from 0.01 to 0.10 after 100 years. Population growth is represented by an annual increase of 1% in traffic demand.

Table 4
Scenarios under mild (scenario 1) and severe (scenario 2) climate change.

Scenario number	Scenario probability	Deterioration rate	Future probability of occurrence*
1	0.5	0.02	0.05
2	0.5	0.04	0.10

* *Note*: The future probability of occurrence indicates the annual probability of occurrence of extreme floods after 100 years.

Based on the preceding description, Table 4 summarizes the two future scenarios that are used for robust traffic assignment. Probabilities are assumed to be 0.5 for both scenarios. As each bridge has two states (safe or failed), there are overall $2^5 = 32$ possible network configurations under traffic and flood hazards. For the sake of simplicity while preserving the conservatism of the estimated risk, independency is assumed among bridge failures as well as failures due to traffic and flood hazards. As a result, the probability of a certain combination of bridge states (e.g. bridge failure pattern) can be determined by the following equation:

$$P_{NET,k} = \sum_{j=1}^{2} P_{FUT,j} \cdot \prod_{i=1}^{5} P_{BR,ijk} \quad (46)$$

where $P_{NET,k}$ is the probability of the k-th combination of bridge states where $k = 1, 2, \cdots, 32$; $P_{FUT,j}$ is the probability of the j-th future scenario; in this example, $P_{FUT,1} = P_{FUT,2} = 0.5$; $P_{BR,ijk}$ is the probability that bridge i is in the state described in combination k given future scenario j; and $P_{BR,ijk}$ can be determined by the following equation:

$$P_{BR,ijk} = \begin{cases} 1 - (1 - P_{f,FLD}) \cdot (1 - P_{f,TR}) & \text{Bridge i fails in Combination k} \\ (1 - P_{f,FLD}) \cdot (1 - P_{f,TR}) & \text{Bridge i survives in Combination k} \end{cases} \quad (47)$$

6.2.4. Results of risk assessment

Based on the future scenarios under climate change and population growth, robust traffic flow patterns can be obtained using the proposed method. Due to traffic supply and demand uncertainties, the robust flow pattern is different from that obtained from deterministic traffic assignment (referred to herein as deterministic flow pattern). Also, the robust flow pattern evolves along with service time due to deterioration and increasing frequency of extreme floods. Fig. 10 shows the deterministic flow pattern and the robust flow patterns after 20, 50, and 100 years. It can be seen that traffic volumes on all links increase considerably due to traffic demand increase and risks posed by climate change. Besides changes of traffic volume on each network link, it is also of interest to investigate the changes in flow ratios among all network links. The ratios of link flows are defined as

$$p_a = \frac{f_a}{\sum_{a \in \mathcal{A}} f_a} \quad (48)$$

where f_a and p_a are the link flow and the link flow ratio associated with link a, respectively. Changes in link flow ratios shed light on the variation of traffic usage in the network as a result of climate change and population growth. For the network considered herein, the comparison of flow ratios, as presented in Fig. 11, shows that the flow ratio diverges considerably from the deterministic flow ratio. This divergence implies that traffic users' route choices change due to climate change and demand increase. For instance, Walt Whitman Bridge and Betsy Ross Bridge (see Fig. 9) are taking over vehicles from Benjamin Franklin Bridge in order to accommodate the increasing demand and to avoid the potential risk of failing bridges on the route passing Benjamin Franklin Bridge (i.e. link 3–4).

Based on the robust flow pattern in each year, the societal risk of the network under climate change and population growth can be assessed using Eq. (40). The parameters needed for risk assessment are summarized in Table 5. Fig. 12 shows the life-cycle risk associated with a service life of 100 years. It can be seen that climate change and demand increase pose a significant risk to the transportation network. The proposed method provides an effective tool to quantitatively assess this risk. In addition, the proposed method to obtain robust traffic flow patterns and the associated societal risks is fundamental for risk-based decision-making on climate adaptation of bridges. For instance, following the ranking approach developed in Yang & Frangopol [27], the present method can be leveraged to rank bridge criticality under

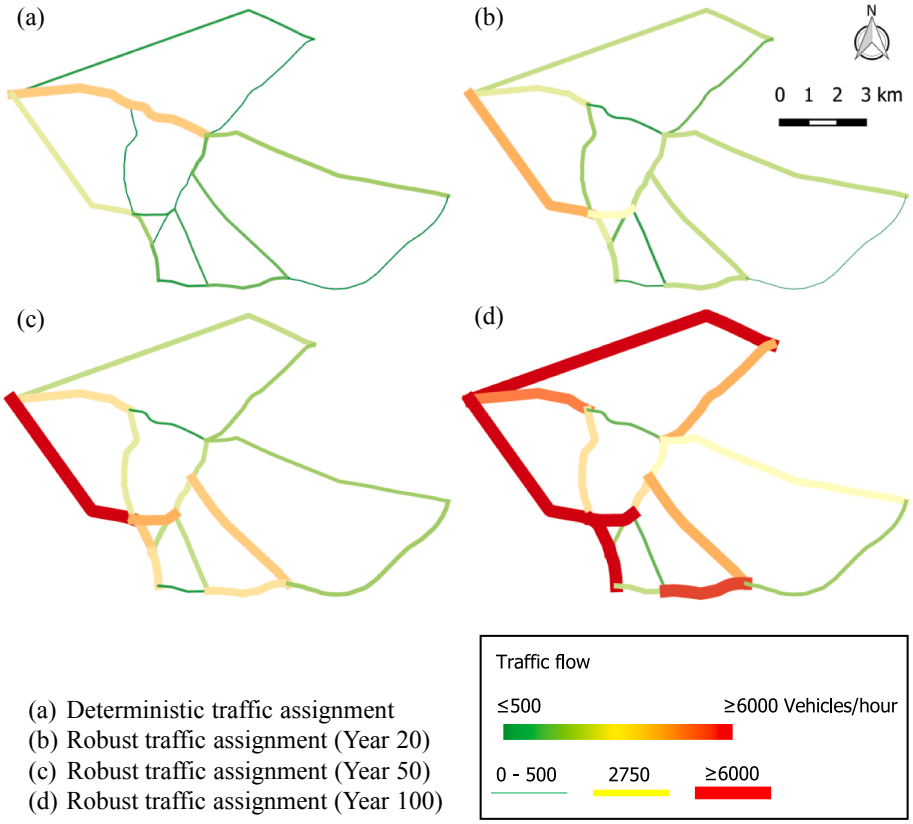

Fig. 10. Traffic flow patterns at different point-in-time.

climate change and population growth. As an advantage over the Monte Carlo-based risk assessment (as in Eq. (39)), the proposed method is capable of providing a robust traffic flow pattern considering supply/demand uncertainties of a transportation network (i.e. scenario uncertainties). Such a pattern can be used in a similar way to the deterministic traffic flow pattern obtained from conventional traffic assignment analysis that does not consider scenario uncertainties. Therefore, climate-informed frameworks for optimal maintenance/rehabilitation planning can potentially be obtained by combining the robust traffic assignment developed herein with either heuristic optimization as in Zhang & Wang [43] or stochastic dynamic programming

Table 5
Parameters in risk analysis [12].

Parameter	Description	Value
α_v	Ratio of average daily truck to average daily traffic	0.12
c_{OT}	Average compensation for truck drivers	26.797 USD/h
O_{car}	Average vehicle occupancies for cars	1.5
O_{truck}	Average vehicle occupancies for trucks	1.05
c_{AW}	Average wage of car drivers	22.82 USD/h
$c_{run,ca}$	Running cost of cars	0.08 USD/km
$c_{run,truck}$	Running cost of trucks	0.375 USD/km
c_{good}	Time value of a cargo	4 USD/h

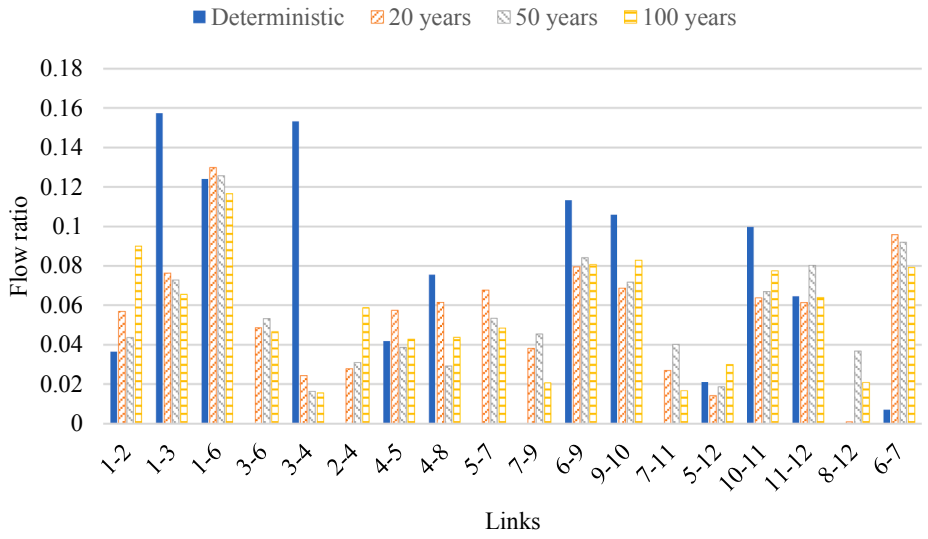

Fig. 11. Traffic flow ratios at different point-in-time.

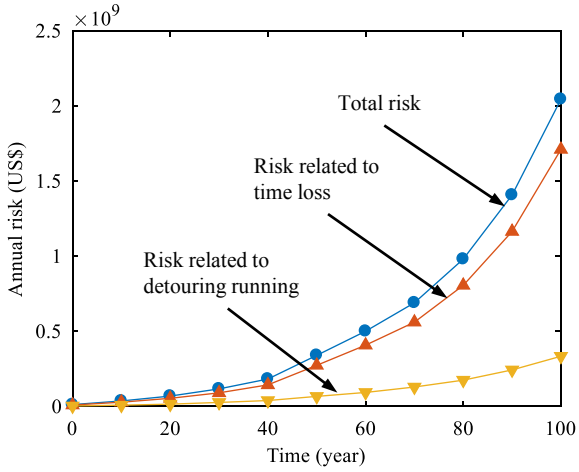

Fig. 12. Life-cycle risk of the Camden-Philadelphia transportation network.

as in Ouyang [9]. Such an integration is outside the scope of this paper and can be pursued in future research.

In Fig. 12, the total annual risk is decomposed to the risk related to time loss and the risk related to detour running. The results in Fig. 12 indicate that the risk related to time loss accounts for a great portion of the total societal risk. This can be expected from the detour data in Table 3, where nearly all bridges have a reasonably short detour length. The aforementioned results showed the combined effect of climate change and population growth on societal risk. It is also important to investigate climate change and population growth separately to compare their impacts on the transportation network. For this purpose, two cases are considered. In the first case, only climate change effects are considered, namely, the OD demands are fixed throughout the time horizon of interest. In the second case, only the traffic demand increase resulting from population growth is considered; in this case, neither traffic nor flood hazards are included in the analysis.

Fig. 13 shows the flow patterns after 50 years obtained from the two cases mentioned above. It can be observed that climate change, through its effects on structural deterioration and flood frequency, can significantly alter the traffic flow pattern in the network. Due to the higher risk associated with traffic and flood hazards on link 3–4, the robust flow pattern in case I (climate change effects only) shows more vehicles on those routes without link 3–4 than the normal condition obtained from deterministic traffic assignment. The divergence from the deterministic flow pattern is less obvious for the flow pattern considering only population growth (case II). Such changes in flow patterns can also be seen from Fig. 14 in terms of link flow ratios. For the 100-year time period under consideration, Fig. 15 presents the societal risk profiles for all three analyzed cases (i.e. risk under climate change only, risk under population growth only, and risk under both climate change and population growth). Based on Figs. 13–15, it is found that the traffic and flood hazards contributes to the alteration of flow patterns, while the demand growth is responsible for the increase in the magnitude of risk. Therefore, when conducting societal risk assessment, climate change and population growth should be considered simultaneously. It should be noted that the results above are related to the network model and the hazard scenarios. Nevertheless, the proposed method provides a general and effective way to assess societal risk of transportation networks under climate change and population growth.

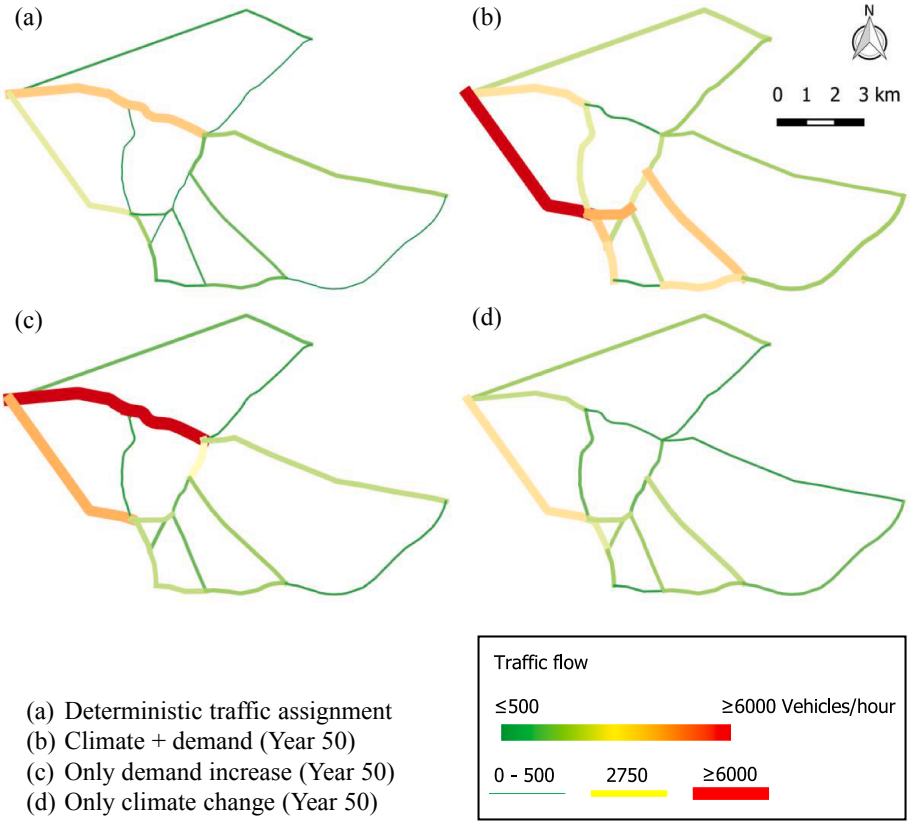

Fig. 13. Flow patterns under different conditions.

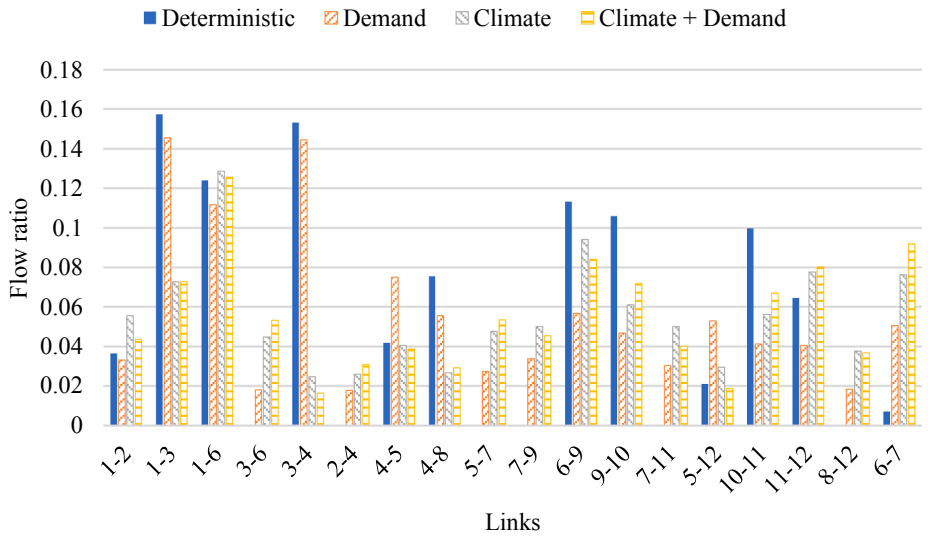

Fig. 14. Flow ratios under different conditions.

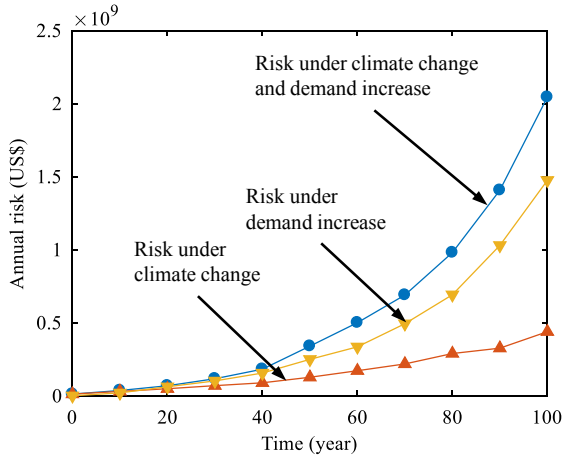

Fig. 15. Life-cycle risk of the Camden-Philadelphia transportation network under different conditions.

7. Conclusions

This paper presents a novel and general method to assess societal risk of transportation networks under uncertainties due to climate change and population growth. Through the identification of future scenarios, the proposed method links uncertainties in climate change and population growth to uncertainties in traffic supply and demand of transportation networks. A robust traffic assignment model based on the expected residual minimization approach is used to obtain robust traffic flow patterns of transportation networks under supply and demand uncertainties. The obtained flow pattern is then used to estimate the societal risk. The proposed method is sufficiently general to consider different network components (e.g. pavements and bridges) and various hazards to transportation networks induced by climate change (e.g. corrosion, hurricanes and flooding).

An efficient algorithm is developed to implement the proposed robust traffic assignment model. The algorithm first uses smoothing method to decompose the nonsmooth objective function to a series of optimization subproblems with smooth objective functions. For each subproblem, quasi-Newton algorithm suitable for large-scale problems (i.e. limited memory BFGS) is used to find the solution efficiently. For cases where the values of objective functions have to be determined with sampling techniques, Latin hypercube sampling is adopted to reduce the required number of samples. In addition, simulated annealing is employed to control the correlation structure of Latin hypercube samples.

The computational efficiency of the proposed method is demonstrated using an example transportation network. The method is also applied to a real-world bridge network located in Camden County, New Jersey, under future climate change and population growth. Based on the results, the following conclusions are drawn:

1. The proposed method is more efficient and numerically robust than existing methods for robust traffic assignment under supply and demand uncertainties. The limited memory Broyden-Fletcher-Goldfarb-Shanno (L-BFGS) algorithm is much more efficient than the projected gradient (PG) algorithm previously used for robust traffic assignment. Compared to the PG algorithm, only a fraction of steps is needed to obtain converged results. Latin hypercube sampling used in the proposed method enables efficient and robust evaluation of objective functions with a much smaller number of samples.
2. Climate change and population growth can significantly proliferate the societal risk imposed upon traffic users in the transportation network. It is shown from the present study that the robust traffic flow pattern obtained using the proposed method can diverge substantially from the deterministic flow pattern. It is also found that hazards affected by climate change can dramatically alter traffic flow patterns in the transportation network, whereas the traffic demand increase due to population growth is responsible for the increase of traffic volume on network links. It is also found that risk associated with time losses accounts for a greater portion of the total societal risk than that associated with running losses.
3. Using the proposed method, climate-informed frameworks for optimal maintenance/rehabilitation planning can potentially be formed by combining the robust traffic assignment developed herein with either heuristic optimization or stochastic dynamic programming. Such an integration has to be pursued in future research.

Acknowledgements

The authors are grateful for the financial support received from the U.S. National Science Foundation Grant CMMI 1537926. The opinions and conclusions presented in this paper are those of the authors and do not necessarily reflect the views of the sponsoring organization.

References

[1] Mondoro A, Frangopol DM, Liu L. Bridge adaptation and management under climate change uncertainties: a review. Nat Hazards Rev, ASCE 2018;19:04017023.
[2] Riahi K, van Vuuren DP, Kriegler E, Edmonds J, O'Neill BC, Fujimori S, et al. The Shared Socioeconomic Pathways and their energy, land use, and greenhouse gas emissions implications: an overview. Global Environ Change 2017;42:153–68.
[3] Bell MGH, Iida Y. Transportation network analysis. Chichester, England: Wiley; 1997.
[4] Daganzo CF, Sheffi Y. On stochastic models of traffic assignment. Transp Sci 1977;11:253–74.
[5] Patriksson M. The traffic assignment problem: models and methods. Mineola, NY: Dover Publications; 2015.
[6] Yazici A, Kamga C, Ozbay K. Evaluation of incident management impacts using stochastic dynamic traffic assignment. Transp Res Procedia 2015;10:186–96.
[7] Kamga CN, Mouskos KC, Paaswell RE. A methodology to estimate travel time using dynamic traffic assignment (DTA) under incident conditions. Transp Res Part C 2011;19:1215–24.
[8] Lam WHK, Shao H, Sumalee A. Modeling impacts of adverse weather conditions on a road network with uncertainties in demand and supply. Transp Res Part B: Methodol 2008;42:890–910.
[9] Ouyang Y. Pavement resurfacing planning for highway networks: parametric policy iteration approach. J Infrastruct Syst, ASCE 2007;13:65–71.
[10] Yin Y, Madanat SM, Lu XY. Robust improvement schemes for road networks under demand uncertainty. Eur J Oper Res 2009;198:470–9.
[11] Bocchini P, Frangopol DM. Generalized bridge network performance analysis with correlation and time-variant reliability. Struct Saf 2011;33:155–64.
[12] Saydam D, Bocchini P, Frangopol DM. Time-dependent risk associated with deterioration of highway bridge networks. Eng Struct 2013;54:221–33.
[13] Saha P, Liu R, Melson C, Boyles SD. Network model for rural roadway tolling with pavement deterioration and repair. Comput-Aided Civ Infrastruct Eng 2014;29:315–29.
[14] Zhou Y, Banerjee S, Shinozuka M. Socio-economic effect of seismic retrofit of bridges for highway transportation networks: a pilot study. Struct Infrastruct Eng 2010;6:145–57.
[15] Bocchini P, Frangopol DM. A stochastic computational framework for the joint transportation network fragility analysis and traffic flow distribution under extreme events. Probab Eng Mech 2011;26:182–93.
[16] Bocchini P, Frangopol DM. Restoration of bridge networks after an earthquake: Multicriteria intervention optimization. Earthquake Spectra 2012;28:427–55.
[17] Frangopol DM, Bocchini P. Bridge network performance, maintenance and optimisation under uncertainty: accomplishments and challenges. Struct Infrastruct Eng 2012;8:341–56.
[18] Zhang C, Chen X, Sumalee A. Robust Wardrop's user equilibrium assignment under stochastic demand and supply: expected residual minimization approach. Transp Res Part B: Methodol 2011;45:534–52.
[19] Mondoro A, Frangopol DM, Liu L. Multi-criteria robust optimization framework for bridge adaptation under climate change. Struct Saf 2018;74:14–23.
[20] Bastidas-Arteaga E, Chateauneuf A, Sánchez-Silva M, Bressolette P, Schoefs F. Influence of weather and global warming in chloride ingress into concrete: a stochastic approach. Struct Saf 2010;32:238–49.
[21] Stewart MG, Wang X, Nguyen MN. Climate change impact and risks of concrete infrastructure deterioration. Eng Struct 2011;33:1326–37.
[22] Dong Y, Frangopol DM. Probabilistic time-dependent multihazard life-cycle assessment and resilience of bridges considering climate change. J Perform Constr Facil, ASCE 2016;30:04016034.
[23] Graham DJ, Glaister S. Road traffic demand elasticity estimates: A review. Transport Reviews 2004;24:261–74.
[24] Paterson W, Watanatada T. Relationships between vehicle speed, ride quality, and road roughness. Measuring Road Roughness and Its Effects on User Cost and Comfort 1985:89–110.
[25] Chandra S. Effect of road roughness on capacity of two-lane roads. J Transp Eng 2004;130:360–4.
[26] Lee J, Madanat S, Reger D. Pavement systems reconstruction and resurfacing policies for minimization of life-cycle costs under greenhouse gas emissions constraints. Transp Res Part B: Methodol 2016;93:618–30.
[27] Yang DY, Frangopol DM. Risk-informed bridge ranking at project and network levels. J Infrastruct Syst, ASCE 2018;24:04018018.
[28] Lim H-W, Song J, Kurtz N. Seismic reliability assessment of lifeline networks using clustering-based multi-scale approach. Earthquake Eng Struct Dyn 2015;44:355–69.
[29] Bureau of Public Roads. Traffic Assignment Manual. US Department of Commerce; 1964.
[30] Nocedal J, Wright SJ. Numerical optimization. 2nd ed. Springer; 2006.
[31] Vořechovský M, Novák D. Correlation control in small-sample Monte Carlo type simulations I: a simulated annealing approach. Probab Eng Mech 2009;24:452–62.
[32] Decò A, Frangopol DM. Risk assessment of highway bridges under multiple hazards. J Risk Res 2011;14:1057–89.
[33] Faber MH, Stewart MG. Risk assessment for civil engineering facilities: critical overview and discussion. Reliab Eng Syst Saf 2003;80:173–84.
[34] Bocchini P, Frangopol DM, Deodatis G. A random field based technique for the efficiency enhancement of bridge network life-cycle analysis under uncertainty. Eng Struct 2011;33:3208–17.
[35] FHWA. Census Transportation Planning Products. Federal Highway Administration Website 2000. http://www.fhwa.dot.gov/planning/census_issues/ctpp/ (accessed July 15, 2016).
[36] Decò A, Frangopol DM. Life-cycle risk assessment of spatially distributed aging bridges under seismic and traffic hazards. Earthquake Spectra 2013;29:127–53.
[37] Kerenyi K, Sofu T, Guo J. Hydrodynamic Forces on Inundated Bridge Decks. Federal Highway Administration Report No FHWA-HRT-09-028 2009:48.
[38] U.S. Geological Survey. National Hydrography Geodatabase 2013. http://viewer.nationalmap.gov/viewer/nhd.html?p=nhd (accessed June 20, 2017).
[39] Ataei N, Padgett JE. Probabilistic modeling of bridge deck unseating during hurricane events. J Bridge Eng 2013;18:275–86.
[40] Mondoro A, Frangopol DM, Soliman M. Optimal risk-based management of coastal bridges vulnerable to hurricanes. J Infrastruct Syst, ASCE 2017;23:04016046.
[41] AASHTO. Guide Specifications for Bridges Vulnerable to Coastal Storms. Washington, D.C.: American Association of State Highway and Transportation Officials (AASHTO); 2008.
[42] Kerenyi K, Sofu T, Guo J. Hydrodynamic Forces on Inundated Bridge Decks: Report No. FHWA-HRT-09-028. Washington, D.C.: Federal Highway Administration (FHWA); 2009.
[43] Zhang W, Wang N. Resilience-based risk mitigation for road networks. Struct Saf 2016;62:57–65.
[44] Guidotti R, Gardoni P, Chen Y. Network reliability analysis with link and nodal weights and auxiliary nodes. Struct Saf 2017;65:12–26.
[45] Shoji G, Moriyama T. Evaluation of the structural fragility of a bridge structure subjected to a tsunami wave load. J Nat Disaster Sci 2007;29:73–81.
[46] Frangopol DM, Kong JS, Gharaibeh ES. Reliability-based life-cycle management of highway bridges. J Comput Civ Eng, ASCE 2001;15:27–34.